ISSN 1606-867X (Print)
ISSN 2687-0711 (Online)
Condensed Matter and Interphases
Kondensirovannye Sredy i Mezhfaznye Granitsy
https://journals.vsu.ru/kcmf/

Original articles

Research article
https://doi.org/10.17308/kcmf.2024.26/12226

Preparation and properties of conversion phosphate-containing coatings on magnesium alloys doped with rare earth elements

A. V. Pospelov[1]✉, A. A. Kasach[2], A. R. Tsyganov[1], I. I. Kurilo[1]

[1]Belarusian State Technological University, Department of Physical, Colloid, and Analytical Chemistry, 13a Sverdlova ul., Minsk 220006, Republic of Belarus

[2]Belarusian State Technological University, Department of Chemistry, Technology of Electrochemical Production and Electronic Engineering Materials, 13a Sverdlova ul., Minsk 220006, Republic of Belarus

Abstract

The purpose of our study was to synthesize and analyze the structure, qualitative and quantitative composition, and protective properties of phosphate-containing conversion coatings on WE43, ZRE1, and QE22 magnesium alloys doped with rare earth elements in the Hank's Balanced Salt Solution.

Scanning electron microscopy, energy dispersive X-ray analysis, and X-ray phase analysis methods were used to study the morphology, microstructure, the elemental and phase compositions of QE22, ZRE1, and WE43 magnesium alloys doped with rare earth elements, as well as conversion coatings formed on their surface during phosphating. Linear voltammetry and electrochemical impedance spectroscopy were used to study the kinetic properties of corrosion of the analyzed samples in the Hank's Balanced Salt Solution (pH = 7.4) imitating the human body environment before and after phosphating.

The study showed that the phosphating of magnesium alloys doped with rare earth elements results in the formation of low-soluble fine-grained coatings with a pronounced crystal structure and a thickness from 16 to 21 μm. The obtained conversion coatings are characterized by the following elemental composition: Ca ≈ 40 wt.%; P ≈ 15 wt.%; and O ≈ 35 wt.%. The crystal structure of phosphate-containing coatings is presented by the brushite phase ($CaHPO_4 \cdot 2H_2O$).

The electrochemical studies of the corrosion behavior of magnesium alloys in the model Hank's Balanced Salt Solution (pH = 7.4) demonstrated that the corrosion current density decreases in the sequence QE22, ZRE1, WE43 and is i_{corr}, A/cm^2: $5.2 \cdot 10^{-5}$; $2.5 \cdot 10^{-5}$; $2.0 \cdot 10^{-5}$. The obtained conversion coatings based on brushite reduce the corrosion rate of QE22, ZRE1, and WE43 magnesium alloys by 15.2, 7.8, and 6.3 times, respectively.

Keywords: Magnesium, Rare earth elements, Conversion coating, Brushite, Corrosion

Funding: The study was funded by the Ministry of Education of the Republic of Belarus as part of the State Research Program "Mechanics, metallurgy, and diagnostics in machinery construction" (2021–2023), subprogram "Electroplating", order No. 4.08: "Obtaining implant materials based on titanium alloys and biodegradable magnesium alloys with enhanced anticorrosive and biocidal properties" (state registration No. 20212333).

Acknowledgements: studies using scanning electron microscopy were carried out using the equipment of the Centre for Physico-Chemical Research Methods of the Belarusian State Technological University.

For citation: Paspelau A. V., Kasach A. A., Tsyganov A. R., Kurilo I. I. Preparation and properties of conversion phosphate-containing coatings on magnesium alloys doped with rare earth elements. *Condensed Matter and Interphases.* 2024;26(3): 504–517. https://doi.org/10.17308/kcmf.2024.26/12226

Для цитирования: Поспелов А.В., Касач А.А., Цыганов А.Р., Курило И.И. Получение и свойства конверсионных фосфатсодержащих покрытий на легированных редкоземельными элементами сплавах магния. *Конденсированные среды и межфазные границы*. 2024; 26(3): 504–517. https://doi.org/10.17308/kcmf.2024.26/12226

✉ Andrei V. Paspelau, e-mail: andrei29088@mail.ru

1. Introduction

Lately, a lot of attention has been paid to biodegradable magnesium alloys in medical applications [1,2]. Construction materials based on magnesium and its alloys have low density, which is close to the density of human bones, and are compatible with the human body [3]. Magnesium is an active metal, so its corrosion in aqueous environments as accompanied by the release of large amounts of hydrogen. Due to abrupt and inhomogeneous corrosion in living organisms, magnesium has limited applications in the production of orthopedic implants. To enhance the mechanical properties and corrosion resistance, magnesium is alloyed with other metals (Zn, Al, Mn, Nd, Ce, Y, Ca, etc.) [4,5]. However, at higher concentrations of alloying additives, especially Al, Zn, and rare earth elements (REE), the corrosion resistance and biocompatibility of magnesium alloys can decrease, and the corrosion products can become more toxic [6–8].

Various physical (laser treatment, magnetron sputtering, intensive plastic deformation) [12–14], chemical (conversion coatings) [15–20], and electrochemical (plasma electrolytic oxidation, electrophoretic deposition) [21–25] methods of surface treatment, as well as biopolymer based coatings [9–11] are used to increase the corrosion resistance and biocompatibility of magnesium alloys. These methods include chemical deposition of conversion coatings, which is the easiest and the most available method that can be used for the treatment of items with complex geometry. Chemical treatment allows obtaining conversion coatings based on magnesium fluorides [16, 17, 26], zinc phosphates [27, 28], strontium [18], magnesium [28, 29], and calcium [15, 28, 30–32].

Obtaining conversion coatings based on magnesium fluorides is environmentally hazardous, because it involves using 20–40% solution of HF, whose vapors cause irritation of the respiratory system, eyes, and skin. In terms of the environment and economy, the most practical method of obtaining conversion coatings is based on phosphates of bioactive materials (Ca, Mg, Zn). Materials based on dicalcium phosphate-dihydrate corresponding to the crystal structure of brushite, are not toxic, have a high biocompatibility, demonstrate osteoconductive properties, and can be integrated into the bone matrix during bone remodeling, which facilitates the osseointegration of implants [33, 34]. The protective properties of conversion coatings based on $CaHPO_4 \cdot 2H_2O$ depend on the microstructure and porosity. Conversion coatings with the highest density and anticorrosive properties are formed, when the pH of the phosphating agent is ≈2.8–3.5 and the temperature is 37–70 °C [15, 35–38]. The synthesis and the protective properties of this type of conversion coatings are well-studied for pure magnesium [15,38] and alloys based on Mg-Al-Zn (AZ series) [28, 30–32, 35–37]. These coatings can reduce the corrosion rate of magnesium alloys doped with aluminum and zinc in model biological environments by 62 times [28]. It is known, however, that aluminum has adverse effect on neurons [39] and osteoblasts [40], and is associated with dementia and Alzheimer's disease [39]. Magnesium alloys containing rare earth elements (REE) are of a significant interest for basic and applied research aimed at synthesizing biodegradable materials. These alloys have good strength and biocompatibility. Modification of the surface of these alloys with brushite based conversion coatings increases their corrosion resistance in the human body and reduces cytotoxicity of the surface of implants.

The purpose of our study was to synthesize and analyze the structure, qualitative and quantitative composition, and protective properties of phosphate-containing conversion coatings on WE43, ZRE1, and QE22 magnesium alloys doped with rare earth elements in the Hank's Balanced Salt Solution.

2. Experimental

In our experiments we used samples of QE22, ZRE1, and WE43 magnesium alloys whose nominal compositions are presented in Table 1.

The samples were cut into 30×20×5 mm^3 pieces, which were then polished with sandpaper (P1000 and P2000) in 96% ethanol.

To obtain phosphate-containing conversion coatings, we used a solution with the following composition, mol/dm^3: $Ca(NO_3)_2$ – 0.2; H_3PO_4 – 0.3. The pH of the solution was raised to 3.0±0.1 by adding 3 M of a NaOH solution. The coatings were deposited for 60 minutes at a temperature of 70 ± 2 °C.

Table 1. Elemental composition of the studied magnesium alloys

Content in alloy, wt.%							
Alloy ZRE1							
Zn	РЗЭ	Zr	Si	Cu	Mn	Ni	Mg
2.7	3.18	0.53	0.01	0.01	0.2	0.001	balance
Alloy QE22							
Ag	Nd		Zr	Cu		Ni	Mg
2.0–3.0	1.7–2.5		0.4–1.0	0.1		0.01	balance
Alloy WE43							
Y	Nd		РЗЭ	Zr			Mg
3.7	3.2		0.96	0.51			balance

The morphology and microstructure of the surface of the obtained coatings were studied using a JSM-5610 LV scanning electron microscope (Jeol), with an EDX JED-2201 energy-dispersive X-ray spectrometer (Jeol Ltd.). The phase composition of the analyzed samples was determined using a D8 Advance X-ray diffractometer (Bruker AXS). The cathode material was Cu ($K\alpha$-1.5406 Å). The diffraction patterns were recorded in the range of 2θ from 5 to 80° with the scanning step of 0.05 °/s. The phases were identified using Match software based on the location and the relative intensity of the registered peaks using the COD (Crystallography Open Database) reference base.

The corrosion behavior of the samples of magnesium alloys was studied in the Hank's Balanced Salt Solution of the following composition, g/dm^3: NaCl – 8; KCl – 0.2; $CaCl_2$ – 0.14; $MgSO_4 \cdot 7H_2O$ – 0.1; $MgCl_2 \cdot 7H_2O$ – 0.10; $Na_2HPO_4 \cdot 2H_2O$ – 0.06; KH_2PO_4 – 0.06; $NaHCO_3$ – 0.35; pH – 7.4.

The electrochemical studies were carried out using an Autolab PGSTAT 302N potentiostat/galvanostat with an FRA 32N impedance spectroscopy unit in a three-electrode cell with the working electrode placed on the side. The geometric area of the working electrode was 1 cm^2. The reference electrode was a saturated silver chloride, the counter electrode was a platinum electrode. The stationary potential was established over 30 min. The potentiodynamic polarization curves were registered in the potential range from –200 mV to +200 mV with regard to the stationary potential at a linear potential sweep rate of 1 mV/s. The impedance spectra were measured at a stationary potential in the frequency range from 10^5 to 10^{-2} Hz. The stabilization of the stationary potential took 30 min. The analysis of the spectra, the selection of the equivalent circuit, and the calculation of the parameters and their elements were performed using ZView. All electrochemical studies were carried out at least three times.

3. Results and discussion

Fig. 1 presents SEM images of the surface of magnesium alloys without (Fig. 1a–c) and with (Fig. 1d–f) conversion coatings. The structures of QE22 (Fig. 1a), ZRE1 (Fig. 1B), and WE43 (Fig. 1c) alloys include regions characteristic for intermetallic particles. Table 2 presents the results of the EDX point analysis of the surface of the initial samples. They demonstrate that the QE22 alloy consists of a magnesium matrix and intermetallic particles enriched in neodymium (27.3 wt.%), silver (8.5 wt.%), and an insignificant amount of zirconium (0.4 wt.%). The intermetallic particles of the ZRE1 alloy contain mainly zinc (19.1 wt.%) and cerium (9.9 wt.%). The magnesium matrix of the WE43 alloy contains up to 5.6 wt.% of neodymium, whose presence can be accounted for by the thermal treatment of the alloy during the preparation process. As compared to other alloys, WE43 is characterized by smaller intermetallic particles whose width and length vary from 10 to 70 μm. The intermetallic particles of this alloy contain ≈ 20 wt.% of neodymium, ≈ 4.5 wt.% of yttrium, ≈ 1 wt.% of praseodymium, and ≈ 0.5 wt.% of cerium (Table 2).

The chemical treatment of the samples of magnesium alloys results in the formation of granular and rough coatings on their surface

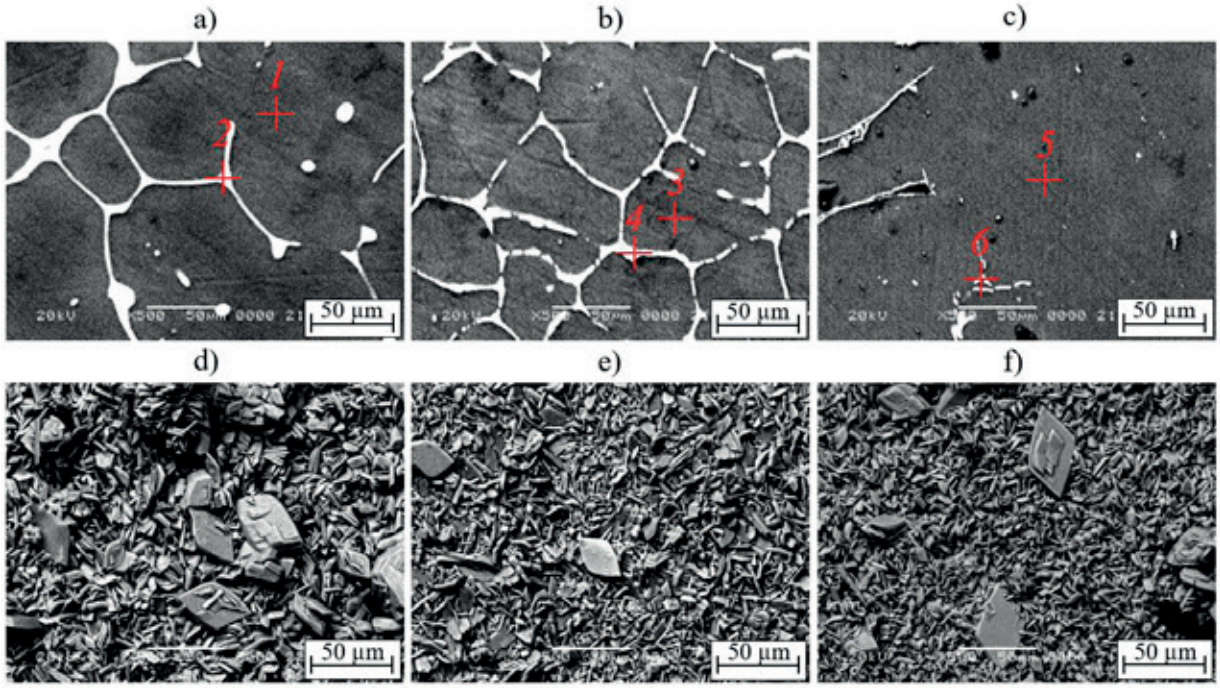

Fig. 1. SEM images of the surface of magnesium alloys without (Fig. 1a–c) and with (Fig. 1d–f) conversion coatings. Alloy: a, d – QE22; b, e – ZRE1; c, f – WE43

Table 2. Results of the point elemental analysis of the initial magnesium alloy samples (the analyzed regions are denoted in Fig. 1)

Number point	Content, wt.%								
	Mg	Zr	Ag	Nd	Zn	Pr	Ce	La	Y
1	100.0	–	–	–	–	–	–	–	–
2	63.8	0.4	8.5	27.3	–	–	–	–	–
3	100.0	–	–	–	–	–	–	–	–
4	63.1	1.3	–	1.8	19.1	0.8	9.9	4.1	–
5	94.4	–	–	5.6	–	–	–	–	–
6	71.4	–	–	21.1	–	1.3	0.6	–	4.6

(Fig. 1e–f). The obtained data demonstrates that conversion coatings on the QE22 alloy have the most inhomogeneous structure (Fig. 1e). This can be explained by the presence of silver, which has a low reactivity.

The obtained conversion coatings consist mainly of calcium, phosphorus, and oxygen, which indicates the formation of phosphate-containing films. Table 3 presents the results of the EDX analysis of the surface of the samples with conversion coatings.

Fig. 2 demonstrates the SEM images and elemental mapping of sections of the studied samples after phosphate conversion coating. They show that the thickness of the conversion coatings on the surface of the studied alloys varies from 16 to 21 μm. The coatings consist of calcium and phosphorus.

The coating on the surface of the QE22 alloy is more inhomogeneous and has microcracks (Fig. 2a). The formation of an inhomogeneous coating with a large number of defects (microcracks) on the surface of QE22 can be explained by the presence of intermetallic particles with a high concentration of silver of up to 8.5 wt.% (Table 2). The increased defectiveness of the obtained coating can be explained by the fact that silver, as compared to magnesium, has a significantly higher standard electrode potential and is chemically stable in acidic environments without oxidizers (including in H_3PO_4 solutions). Therefore, during the formation of conversion

Table 3. Elemental composition of the phosphated magnesium alloys

Alloy	Content, wt.%								
	O	P	Ca	Y	Zn	Zr	La	Ce	Nd
QE22	35.3	15.5	45.1	–	–	4.1	–	–	–
ZRE1	38.3	15.1	40.8	–	1.3	2.4	0.9	1.2	–
WE43	36.4	13.8	40.9	1.5	–	4.0	1.4	0.9	1.1

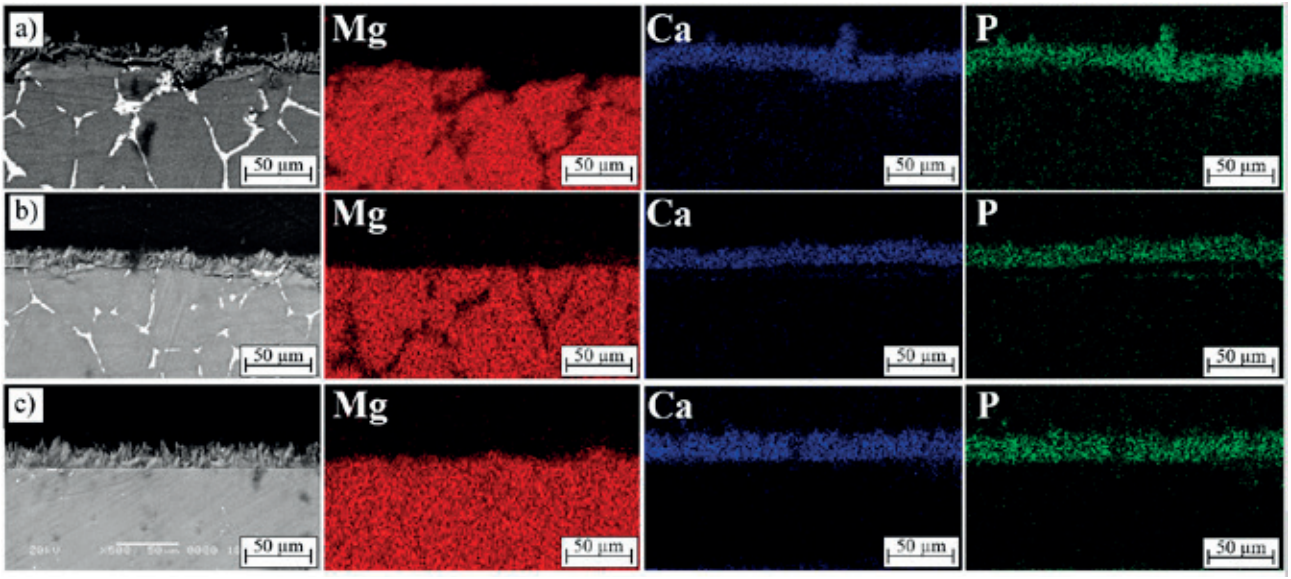

Fig. 2. SEM images and elemental mapping of sections of the studied samples after phosphate conversion coating. Alloy: a – QE22; b – ZRE1; c – WE43

coatings, regions with high concentrations of silver act as cathodes. The reduction of the depolarizer (hydrogen) takes place on their surface. Magnesium ionization takes place in the regions adjacent to silver-containing intermetallic particles.

An increased rate of the local dissolution of the magnesium matrix around the cathode particles (phase $Mg_{12}Nd_2Ag$) and the resulting intensification of hydrogen evolution on intermetallic particles lead to the formation of loose phosphate-containing coatings with a significant number of structural defects (Fig. 2a). The formed conversion coatings limit contacts between the corrosive environment and the metal substrate thus reducing the corrosion rate of the QE22 alloy. However, the presence of defects around the cathode intermetallic particles results in underfilm corrosion and delamination of the coating.

Using X-ray diffraction, we determined the phase composition of the studied samples (Fig. 3). Rare earth elements are known to have low solubility in magnesium. Therefore, their crystallization is accompanied by the formation of separate phases, which enhance the strength characteristics of the alloy [41, 42]. According to the obtained data (Fig. 3a, b), $Mg_{12}Nd_2Ag$ and $(Mg, Zn)_{12}$ intermetallic particles are formed in the compositions of QE22 and ZRE1 alloys respectively, which agrees well with the literature data [41, 42]. The diffraction patterns of the WE43 alloy did not show any intense peaks characteristic for $Mg_{12}Nd$ and $Mg_{12}Nd_2Y$. The diffraction peaks of the a-Mg phase for WE43 (Fig. 3c) are shifted towards smaller angles 2θ as compared to the diffraction peaks of α-Mg for QE22 and ZRE1. This shift indicates an increase in the interplanar distance due to the inclusion of Nd atoms in the crystal lattice of magnesium and the formation of a solid substitution solution, which is confirmed by the results of the EDX analysis.

The diffraction patterns of all the studied alloys with conversion coatings demonstrated

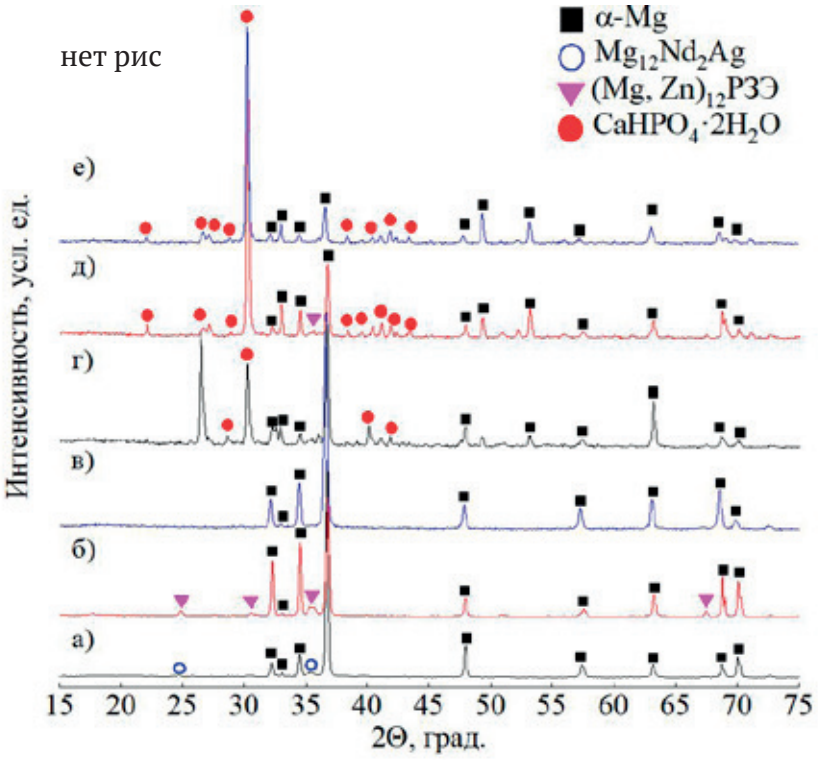

Fig. 3. Diffraction patterns of the surface of magnesium alloys without (Fig. 1a–c) and with (Fig. 1d–f) conversion coatings. Alloy: a, d – QE22; b, e – ZRE1; c, f – WE43

peaks corresponding to the $CaHPO_4 \cdot 2H_2O$ phase (Fig. 3d-f).

The formation of dicalcium phosphate dihydrate during the preparation of conversion coatings can be explained by the following. When magnesium alloy samples are put into the phosphating agent with a slightly acidic pH, intensive dissolution of magnesium is observed, which is accompanied by the release of hydrogen and a local increase in the pH on the electrode|electrolyte interface:

$$Mg \rightarrow Mg^{2+} + 2e^- \text{ (anodic reaction)} \quad (1)$$

$$2H^+ + 2e^- \rightarrow H_2 \text{ (cathodic reaction)} \quad (2)$$

Local alkalization of the electrolyte contacting the surface of magnesium alloys facilitates the formation of a surface layer consisting mainly of $CaHPO_4 \cdot 2H_2O$, according to the following reaction:

$$Ca^{2+} + H_2PO_4^- + 2H_2O \rightarrow CaHPO_4 \cdot 2H_2O + H^+ \quad (3)$$

Fig. 4 shows the potentiodynamic polarization curves of the magnesium alloy samples in Hank's Balanced Salt Solution, and Table 4 presents the electrochemical parameters of corrosion of the studied alloys calculated based on the results of electrochemical polarization. The anodic polarization curve (PC) of QE22 in the potential range from –1.3 to –1.2 V demonstrates a linear region which corresponds to active dissolution of the alloy. The anodic polarization curves of ZRE1 and WE43 in the potential ranges of –1.35 – (–1.30) V and –1.4 – (–1.35) V respectively demonstrate an active-passive region whose presence might indicate the formation of a dense layer of corrosion products. The abrupt change in the angular coefficient b_a of the anodic PC observed when the potential shifted further towards positive values, can be explained by the breakdown of the formed oxide-hydroxide layer and the beginning of active dissolution of the alloy. Regardless of the composition of magnesium alloys, the cathodic PCs have practically the same slope angle, and the cathodic coefficient $|b_к|$ varies in the range from 0.25 to 0.27 V. This indicates that cathodic processes accompanying the corrosion of the studied alloys are of the same type.

According to the obtained results, QE22 (corrosion current density $5.2 \cdot 10^{-5}$ A/cm^2)

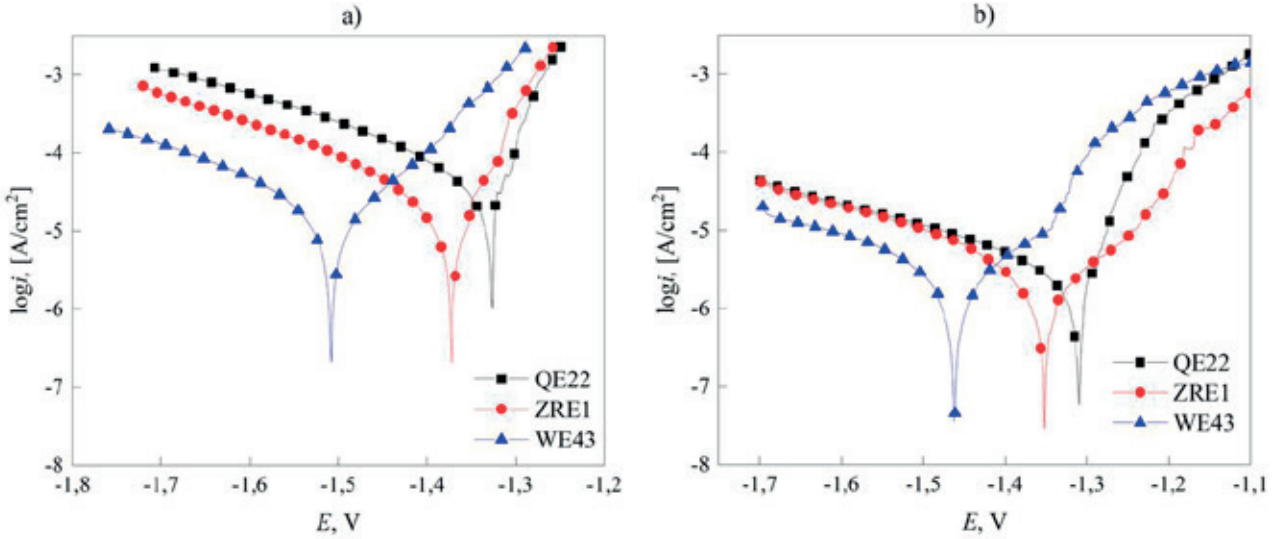

Fig. 4. Polarization curves of magnesium alloys without (a) and with (b) conversion coatings.

Table 4. Electrochemical parameters of corrosion of the magnesium alloy samples

Sample	$\|b_к\|$, V	$\|a_к\|$, V	$\|b_a\|$, V	$\|a_a\|$, V	i_{corr}, A/cm²
Initial alloy samples					
QE22	0.27	2.46	0.09	0.95	$5.2\cdot10^{-5}$
ZRE1	0.25	2.51	0.07	1.01	$2.5\cdot10^{-5}$
WE43	0.27	2.70	0.10	0.97	$2.0\cdot10^{-5}$
Conversion coated alloys					
QE22	0.33	3.14	0.07	0.99	$3.4\cdot10^{-6}$
ZRE1	0.36	3.29	0.17	0.41	$3.3\cdot10^{-6}$
WE43	0.35	3.38	0.17	0.52	$3.2\cdot10^{-6}$

demonstrated the lowest corrosion resistance in Hank's Balanced Salt Solution. The WE43 alloy has a 2.6 and 1.25 times lower corrosion resistance than QE22 and ZRE1 respectively.

Conversion coatings reduce the corrosion rate of QE22, ZRE1, and WE43 by 15.2, 7.8, and 6.3 times respectively. The anodic PCs of ZRE1 and WE43 demonstrate a significant growth of the active-passive region and an increase in the angular coefficient b_a, which indicated the inhibition of anodic processes. Despite similar corrosion current densities of the studied alloys with conversion coatings, the kinetics of the anodic process of QE22 in Hank's Balanced Salt Solution differs significantly from those of ZRE1 and WE43. The slope angle of the anodic PC of QE22 after phosphating remains practically unchanged, which can indicate a low protective ability of the formed conversion coating.

he method of electrochemical impedance spectroscopy was used for a more detailed study of the corrosion processes in the studied samples in Hank's Balanced Salt Solution. The impedance spectra of the magnesium samples presented as Nyquist diagrams demonstrate three time constants: capacitive semicircles in the region of high and low frequencies and an inductive loop in the region of low frequencies (Fig. 5). The capacitive semicircle in the region of high frequencies characterizes the charge transfer through the layer of corrosion products, and the capacitive semicircle in the region of low frequencies reflects the relaxation mass transfer processes in the solid phase as well as the charge transfer resistance in the double electric layer. The low-frequency inductive response indicates active ionization of the electrode.

Conversion coatings based on $CaHPO_4\cdot2H_2O$ increase the values of the impedance modulus of the studied alloys, which is demonstrated by

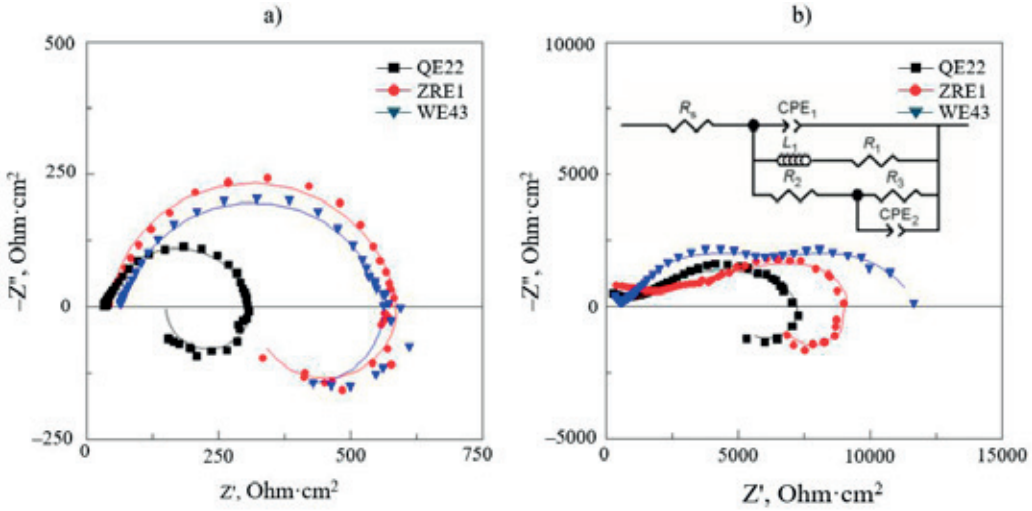

Fig. 5. Impedance spectra of the magnesium alloys presented as Nyquist diagrams without (a) and with (b) conversion coatings.

increase diameters of the capacitive semicircles. The impedance spectra of the QE22 and ZRE1 samples demonstrate an inductive loop in the region of low frequencies. The presence of the loop in the electrochemical impedance spectra of the alloys with conversion coatings might indicate the defectiveness of the formed coating and ionization of magnesium under the formed layer of $CaHPO_4 \cdot 2H_2O$. The impedance hodographs of the WE43 alloy with a conversion coating is characterized by the lack of inductive loops in region of low frequencies, which can be accounted for by the integrity of the formed coating.

An equivalent circuit presented in Fig. 5b was used for the quantitative description of the obtained impedance spectra. In the suggested circuit R_s is the resistance of the electrolyte; R_1 is the resistance of the corrosion products layer; L is the inductance parameter; R_2 is the surface resistance; CPE_1 is the capacitive response of the corrosion products layer; and R_3 is the charge transfer resistance; CPE_2 is the capacitive response of the electrical double layer. Due to the lack of induction processes, they were not used for the quantitative description of the impedance spectra of the WE43 alloy with a conversion coating.

The obtained results demonstrate that WE43 with a conversion coating has the highest corrosion resistance in Hank's Balanced Salt Solution. The obtained results are in good agreement with the data obtained by means of linear polarization.

Corrosion of magnesium alloys as accompanied by the release of hydrogen gas, which increases the pH of solutions. Therefore, it is practical to perform a comparative analysis of the protective abilities of the obtained coatings based on the dynamics of the pH of the corrosive environment

Table 5. Selection of the equivalent circuit

Grade alloy	R_s, Ohm·cm²	CPE1, 10^{-5} Ohm^{-1}·cm^{-2}·c^n	n_1	L, kN	R_1, kOhm·cm²	R_2, kOhm·cm²	CPE2, 10^{-4} Ohm^{-1}·cm^{-2}·c^n	n_2	R_3, Ом·см²
Initial alloy samples									
QE22	42.1	2.2	0.91	5.44	0.55	0.54	30.0	0.90	13
ZRE1	32.0	2.8	0.90	1.71	0.17	0.23	40.4	0.30	75
WE43	65.7	5.0	0.85	13.76	0.35	0.50	3.0	0.90	15
Conversion coated alloys									
QE22	48.0	4.4	0.80	190.50	12.90	0.93	0.25	0.48	6902
ZRE1	90.0	9.1	0.20	50.00	11.00	0.60	0.14	0.60	47361
WE43	496.7	1.1	0.65	–	6.90	4.38	1.86	0.73	–

in contact with the studied samples.

Fig. 6 demonstrates dependences of the pH of Hank's Balanced Salt Solution on the time of exposure of the initial magnesium alloys. The initial pH of Hank's Balanced Salt Solution is 7.4. After keeping the QE22 sample in the solution for 24 hours, the pH fluctuated abruptly and was ≈11. After keeping the QE22 sample in the solution for 7 days, the pH did not grow significantly, which can be explained by the formation of a low-soluble layer of corrosion products – magnesium hydroxide and carbonate. Alloys ZRE1 and WE43 are characterized by a lower corrosion rate in Hank's Balanced Salt Solution. Thus, the pH of the corrosive environments 24 hours after putting ZRE1 and WE43 into them was 9.2 and 9.3, and after 7 days it was 10.1 and 10.0 respectively.

The brushite based conversion coating $CaHPO_4 \cdot 2H_2O$ significantly lowers the alkalization rate of Hank's Balanced Salt Solution with the studied samples. After 24 hours of experimenting with the coated QE22 alloy, the pH of the electrolyte was 8.3, and after 3 days the pH grew rapidly to 11.3, which indicated the beginning of active dissolution of the alloy. When the ZRE1 and WE43 alloys with conversion coatings were used, the pH of Hank's Balanced Salt Solution remained the same after 3 days: 7.5 and 7.6 respectively. A comparative analysis of the dynamics of the pH of corrosive environments with phosphated ZRE1 and WE43 demonstrated that between 3 and 5 days after the beginning of the experiment, the alkalization process was more active in the solution with the WE43 alloy. However, after 7 days, the pH of the corrosive environments became practically identical and were ≈8.4.

Fig. 7 and 8 demonstrate the SEM images of the surface of magnesium alloy samples after their exposure in Hank's Balanced Salt Solution for 24 hours and for 7 days respectively. The surface of the QE22 alloy after 24 hours of corrosion testing was almost completely covered in an inhomogeneous layer of corrosion products, whose structure had macrodefects (Fig. 7a). ZRE1 and WE43 are the least susceptible to corrosion in the first 24 hours of testing, which is explained by the formation of a dense layer of corrosion products preventing further dissolution of the alloys. The QE22 sample almost completely dissolves in Hank's Balanced Salt Solution in 7 days. Increasing the exposure time of the ZRE1 alloy in Hank's Balanced Salt Solution up to 7 days results on the formation of pitting corrosion centers.

The surface of the QE22 sample with a conversion coating demonstrated the formation of pores after 24 hours of exposure in Hank's Balanced Salt Solution. The diameter of the pores varies from 10 to 40 μm. After 7 days of exposure, the surface is covered in a continuous layer of corrosion products and the conversion coating is broken down, which can indicate low protective abilities of the coating resulting

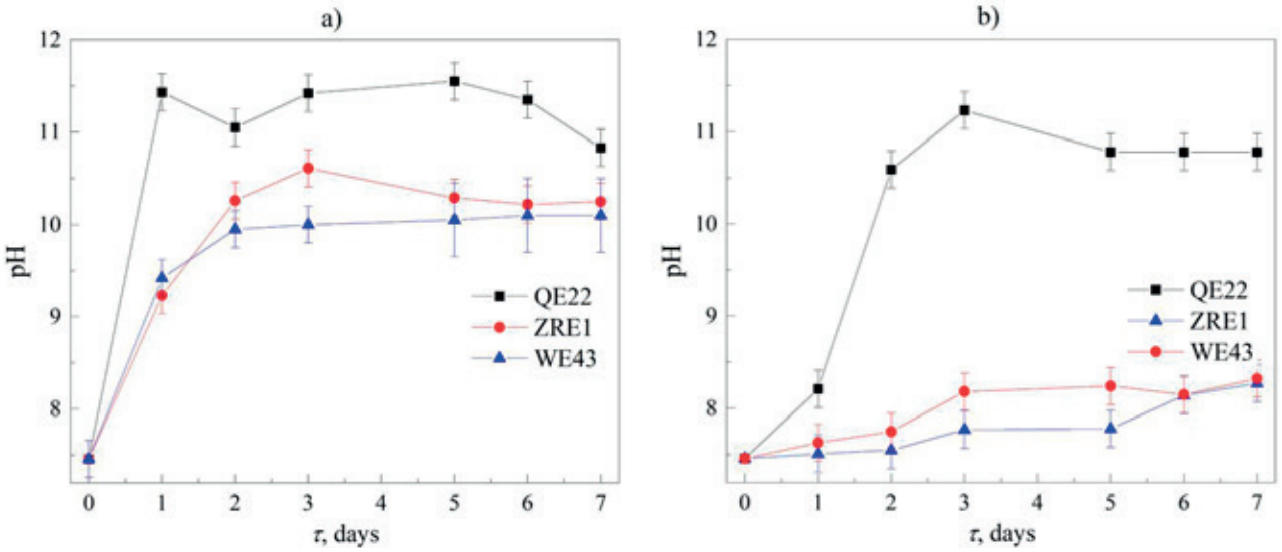

Fig. 6. The dynamics of the pH of Hank's Balanced Salt Solution during corrosion testing of alloys before (a) and after (b) chemical treatment.

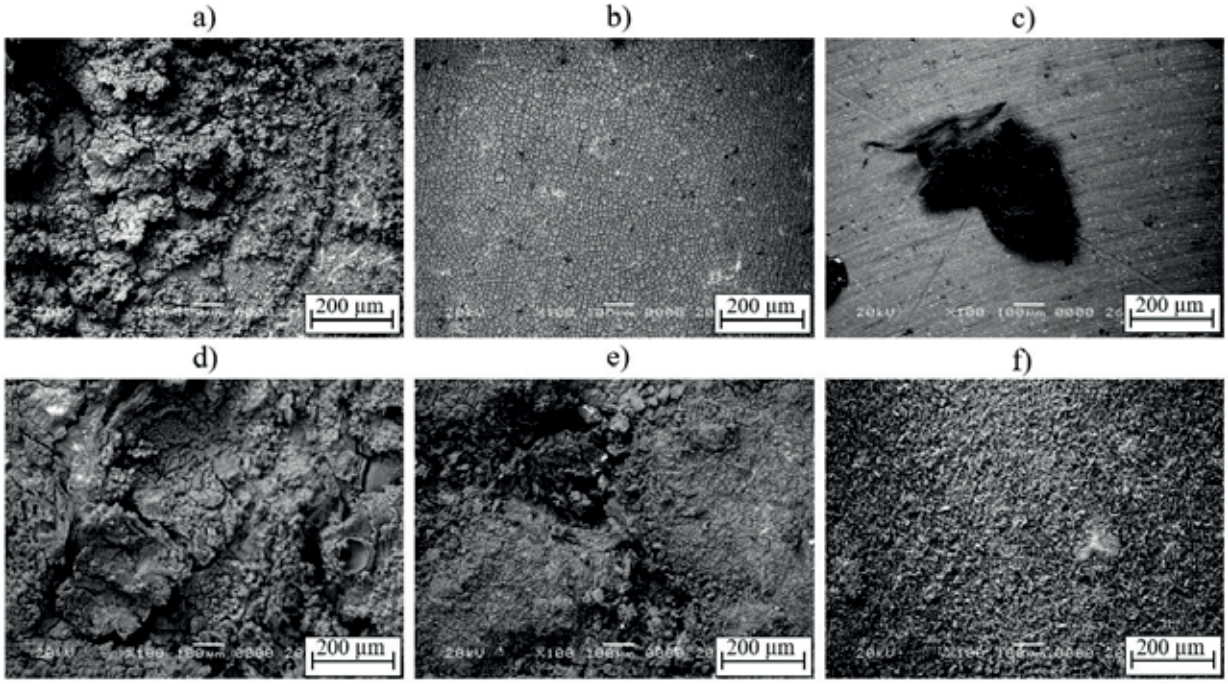

Fig. 7. SEM images of the initial magnesium alloy samples after 24 hours (a-c) and after 7 days (d-f) of corrosion testing in Hank's Balanced Salt Solution. Alloy: a, d – QE22; b, e – ZRE1; c, f – WE43

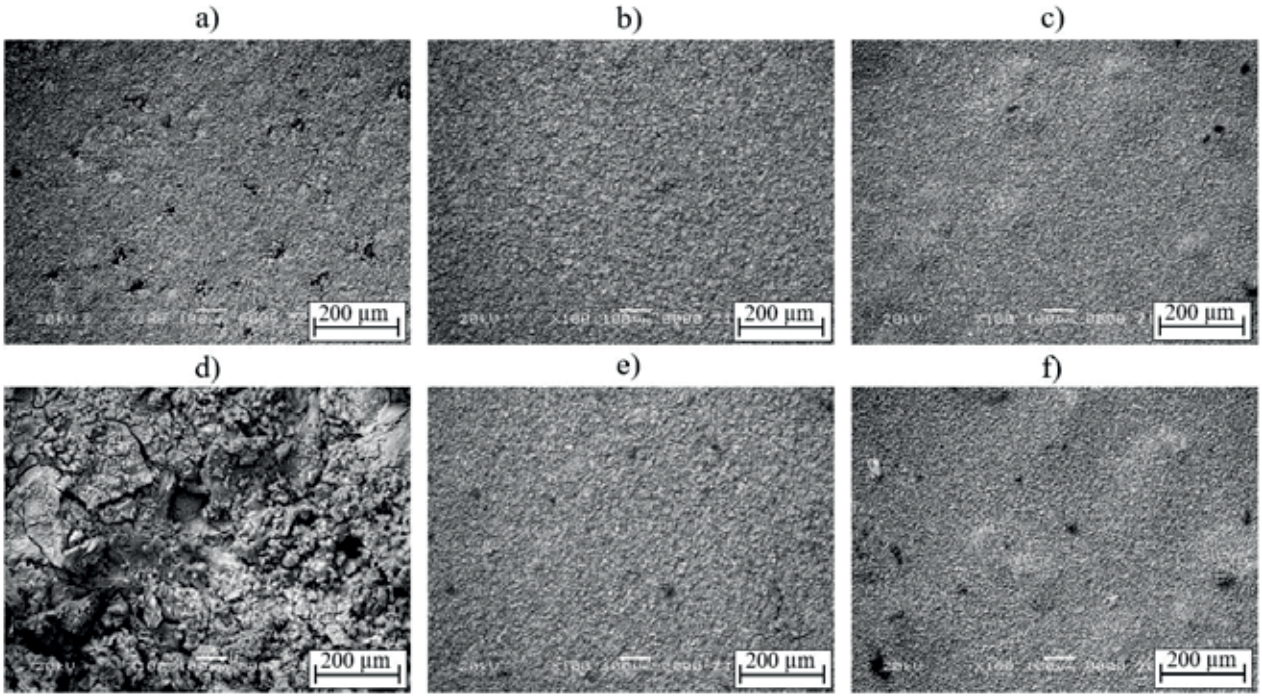

Fig. 8. SEM images of the phosphated magnesium alloy samples after 24 hours (a-c) and after 7 days (d-f) of corrosion testing in Hank's Balanced Salt Solution. Alloy: a, d – QE22; b, e – ZRE1; c, f – WE43

from its inhomogeneity and defectiveness. The microstructure of ZRE1 and WE43 with conversion coatings remains practically the same after 24 hours of corrosion testing in Hank's Balanced Salt Solution. When the time of exposure is increased up to 7 days, an insignificant number of local corrosion centers (pores) are formed on their surface.

Fig. 9 demonstrates the SEM images of the surface of the studied samples with and without

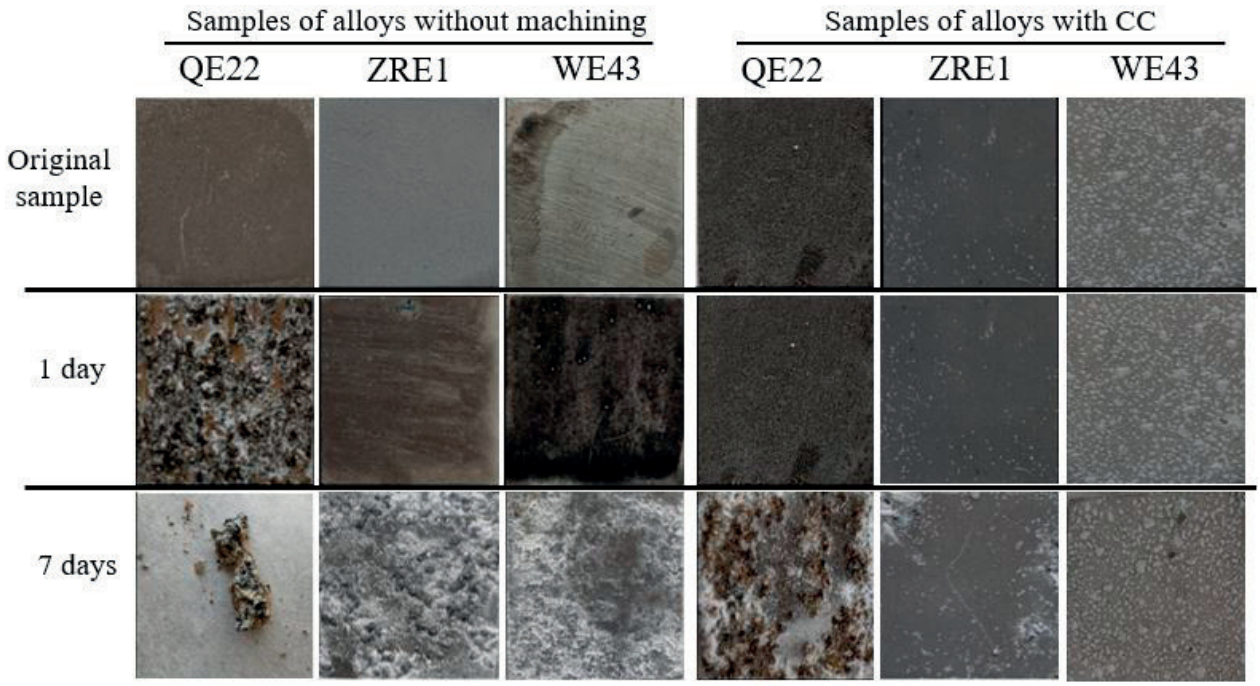

Fig. 9. Images of the surface of magnesium alloy samples after corrosion testing in Hank's Balanced Salt Solution.

conversion coatings after 24 hours and after 7 days of exposure in Hank's Balanced Salt Solution.

After the first 24 hours of corrosion testing, corrosion centers are formed on the surface of the QE22 alloy; the sample completely dissolved in 7 days. Visual assessment of the surface of ZRE1 and WE43 demonstrated that they remained intact after 7 days of testing. The surface of QE22 with a conversion coating does not change significantly after 24 hours of testing. After 7 days of testing, the surface of the alloy was almost completely covered in corrosion products. There were no visible corrosion centers on the surface of coated ZRE1 and WE43 samples after 7 days of testing.

Therefore, conversion coatings based on $CaHPO_4 \cdot 2H_2O$ (brushite) demonstrated a decrease in the corrosion rate of magnesium alloys QE22, ZRE1, and WE43 by 15.2, 7.8, and 6.3 times respectively. The obtained results are in good agreement with those presented in [28,31,32], where similar coatings on magnesium alloys doped with aluminum (series AZ) were demonstrated to reduce the corrosion current density by 19–62 times, while the differences in the protective properties of the conversion coating based on brushite are explained by the impact of the substrate composition on the structure and defectiveness of the formed coatings. Our study confirmed this assumption and stress the importance of the chemical composition and the structure of magnesium alloys when choosing the technique of deposition of conversion coatings. We should note that despite the high effectiveness of protective conversion coatings on magnesium alloys of the AZ series, the use of these alloys as implant materials is associated with risk due to the presence of aluminum. Excessive amounts of aluminum in the human body has an adverse effect on neurons and osteoblasts and can cause Alzheimer's disease, which makes it even more important to carefully choose magnesium alloys for orthopedic implants.

4. Conclusions

Phosphating of magnesium alloys in solutions containing calcium nitrate results in the formation of low-soluble fine-grained coatings with a pronounced crystal structure including Ca ≈ 40 wt.%; P ≈ 15 wt.%; and O ≈ 35 wt.% and consisting mainly of brushite ($CaHPO_4 \cdot 2H_2O$). The coating formed on the surface of QE22 is characterized by highest inhomogeneity and the presence of microcracks, which can be explained by the presence of silver in its composition.

The corrosion resistance of magnesium alloys in Hank's Balanced Salt Solution (pH = 7.4), imitating the environment of the human body, decreases in the sequence QE22, ZRE1, WE43, and the corrosion current density i_{corr} is $5.2 \cdot 10^{-5}$, $2.5 \cdot 10^{-5}$ and $2.0 \cdot 10^{-5}$ A/cm^2, respectively. Conversion coatings reduce the corrosion rate of QE22, ZRE1, and WE43 by 15.2, 7.8, and 6.3 times respectively. Thus, the study demonstrated that conversion coatings formed on WE43 have the best protective abilities. The corrosion testing demonstrated that coated ZRE1 and WE43 alloys can resist corrosion in Hank's Balanced Salt Solution for 7 days without visible damage.

Contribution of the authors

The authors contributed equally to this article.

Conflict of interests

The authors declare that they have no known competing financial interests or personal relationships that could have influenced the work reported in this paper.

References

1. Riaz U., Shabib I., Haider W. The current trends of Mg alloys in biomedical applications – A review. *Journal Biomedical Materials Research – Part B Applied Biomaterials*. 2019;107: 1970–1996. https://doi.org/10.1002/jbm.b.34290

2. Zheng Y. F., Gu X. N., Witte F. Biodegradable metals. *Materials Science Engineering R: Reports*. 2014;77: 1–34. https://doi.org/10.1016/j.mser.2014.01.001

3. Tan J., Ramakrishna S. Applications of magnesium and its alloys : A review. *Applied Sciences*. 2021;11(15): 6861. https://doi.org/10.3390/app11156861

4. Król M. Solidification characteristics of Mg-Li-Al alloys. *Solid State Phenomena*. 2018;275: 41–52. https://doi.org/10.4028/www.scientific.net/SSP.275.41

5. Gusieva K., Davies C. H. J., Scully J. R., Birbilis N. Corrosion of magnesium alloys: The role of alloying. *International Materials Reviews*. 2015;60(3): 169–194. https://doi.org/10.1179/1743280414Y.0000000046

6. Antoniac I. V., Miculescu M., Mănescu V., ... Earar K. Magnesium-based alloys used in orthopedic surgery. *Materials*. 2022;15(3): 1148. https://doi.org/10.3390/ma15031148

7. Gu X., Zheng Y., Cheng Y., Zhong S., Xi T. In vitro corrosion and biocompatibility of binary magnesium alloys. *Biomaterials*. 2029;30(4): 484–498. https://doi.org/10.1016/j.biomaterials.2008.10.021

8. Drynda A., Deinet N., Braun N., Peuster M. Rare earth metals used in biodegradable magnesium-based stents do not interfere with proliferation of smooth muscle cells but do induce the upregulation of inflammatory genes. *Journal of Biomedical Materials Research – Part A*. 2019;91: 360–369. https://doi.org/10.1002/jbm.a.32235

9. Ma Y., Talha M., Wang Q., Zhou N., Li Z., Lin Y. A multifunctional coating with modified calcium phosphate/chitosan for biodegradable magnesium alloys of implants. *New Journal of Chemistry*. 2022;46: 4436–4448. https://doi.org/10.1039/d2nj00147k

10. Kozina I., Krawiec H., Starowicz M., Kawalec M. Corrosion resistance of MgZn alloy covered by chitosan-based coatings. *International Journal Molecular Sciences*. 2021;22 (15): 8301. https://doi.org/10.3390/ijms22158301

11. Huang W., Mei D., Zhang J., ... Guan S. Improved corrosion resistance and cytocompatibility of Mg–Zn–Y–Nd alloy by the electrografted polycaprolactone coating. *Colloids Surfaces A: Physicochemical Engineering Aspects*. 2021;629: 127471. https://doi.org/10.1016/j.colsurfa.2021.127471

12. Pulido-González N., Torres B., Zheludkevich M. L., Rams J. High Power Diode Laser (HPDL) surface treatments to improve the mechanical properties and the corrosion behaviour of Mg-Zn-Ca alloys for biodegradable implants. *Surface and Coatings Technology*. 2020;402: 126314. https://doi.org/10.1016/j.surfcoat.2020.126314

13. Liu Y., Curioni M., Dong S., Liu Z. Understanding the effects of excimer laser treatment on corrosion behavior of biodegradable Mg-1Ca alloy in simulated body fluid. *Journal of Magnesium and Alloy*. 2021;10(4): 1004–1023. https://doi.org/10.1016/j.jma.2021.11.011

14. Hou S., Yu W., Yang Z., Li Y., Yang L., Lang S. Properties of titanium oxide coating on MgZn alloy by magnetron sputtering for stent application. *Coatings*. 2020;10(10): 1–10. https://doi.org/10.3390/coatings10100999

15. Braga J. de O., Carvalho de S. M., Silva L. M. C., ... Nunes E. H. M. Fabrication and characterization of dicalcium phosphate coatings deposited on magnesium substrates by a chemical conversion route. *Surface and Coatings Technology*. 2020;386: 125505. https://doi.org/10.1016/j.surfcoat.2020.125505

16. Sathyaraj M., Ravichandran K., Narayanan S. Controlling the rate of degradation of Mg using magnesium fluoride and magnesium fluoride-magnesium phosphate duplex coatings. *Journal Magnesium and Alloy*. 2022;10(1): 295–312. https://doi.org/10.1016/j.jma.2021.06.005

17. Cheng S., Wang W., Wang D., ... Zhang Y. An in vitro and in vivo comparison of $Mg(OH)_2$-, MgF_2- and HA-coated Mg in degradation and osteointegration. *Biomaterials Science*. 2020;8: 3320–3333. https://doi.

org/10.1039/d0bm00467g

18. Chen X. B., Nisbet D. R., Li R. W., ... Birbilis N. Controlling initial biodegradation of magnesium by a biocompatible strontium phosphate conversion coating. *Acta Biomaterialia*. 2014;10(3): 1463–1474. https://doi.org/10.1016/j.actbio.2013.11.016

19. Chunyan Z., Shangju L., Baoxing Y., ... Fuhui W. Ratio of total acidity to pH value of coating bath: A new strategy towards phosphate conversion coatings with optimized corrosion resistance for magnesium alloys. *Corrosion Science*. 2019;150: 279–295. https://doi.org/10.1016/j.corsci.2019.01.046

20. Wu Q., Yu B., Zhou P., Zhang T., Wang F. Fabrication of phosphate conversion coatings on rolled AZ31 magnesium alloy: Variation of corrosion resistance on different planes induced by the crystallographic texture. *Materials Chemistry and Physics*. 2021;273: 125121. https://doi.org/10.1016/j.matchemphys.2021.125121

21. Chaharmahali R., Fattah-alhosseini A., Nouri M., Babaei K. Improving surface characteristics of PEO coatings of Mg and its alloys with zirconia nanoparticles: a review. *Applied Surface Science Advances*. 2021;6: 100131. https://doi.org/10.1016/j.apsadv.2021.100131

22. Seyfi M., Fattah-alhosseini A., Pajohi-Alamoti M., Nikoomanzari E. Effect of ZnO nanoparticles addition to PEO coatings on AZ31B Mg alloy: antibacterial effect and corrosion behavior of coatings in Ringer's physiological solution. *Journal of Asian Ceramic Societies*. 2021;9(3): 1114–1127. https://doi.org/10.1080/21870764.2021.1940728

23. Daavari M., Atapour M., Mohedano M., ... Taherizadeh A. Quasi-in vivo corrosion behavior of AZ31B Mg alloy with hybrid MWCNTs-PEO/PCL based coatings. *Journal of Magnesium and Alloys*. 2021;10(11): 3217–3233. https://doi.org/10.1016/j.jma.2021.09.010

24. Taranu B.-O., Ianasi P., Rus S. F., Bucur A. I. Simultaneous precipitation and electrodeposition of hydroxyapatite coatings at different temperatures on various metal substrates. *Coatings*. 2022;12(2): 288. https://doi.org/10.3390/coatings12020288

25. Yuan B., Chen H., Zhao R., ... Zhang X. Construction of a magnesium hydroxide/graphene oxide/hydroxyapatite composite coating on Mg–Ca–Zn–Ag alloy to inhibit bacterial infection and promote bone regeneration. *Bioactive Materials*. 2022;18: 354–367. https://doi.org/10.1016/j.bioactmat.2022.02.030

26. Wang P., Liu J., Shen S., ... Xi T. In vitro and in vivo studies on two-step alkali-fluoride-treated Mg-Zn-Y-Nd alloy for vascular stent application: Enhancement in corrosion resistance and biocompatibility. *ACS Biomaterials Science and Engineering*. 2019;5(7): 3279–3292. https://doi.org/10.1021/acsbiomaterials.9b00140

27. Van Phuong N., Moon S. Comparative corrosion study of zinc phosphate and magnesium phosphate conversion coatings on AZ31 Mg alloy. *Materials Letters*. 2014;122: 341–344. https://doi.org/10.1016/j.matlet.2014.02.065

28. Zai W., Zhang X., Su Y., Man H.C., Li G., Lian J. Comparison of corrosion resistance and biocompatibility of magnesium phosphate (MgP), zinc phosphate (ZnP) and calcium phosphate (CaP) conversion coatings on Mg alloy. *Surface and Coatings Technology*. 2020;397: 125919. https://doi.org/10.1016/j.surfcoat.2020.125919

29. Ishizaki T., Shigematsu I., Saito N. Anticorrosive magnesium phosphate coating on AZ31 magnesium alloy. *Surface and Coatings Technology*. 2009;203(16): 2288–2291. https://doi.org/10.1016/j.surfcoat.2009.02.026

30. Su Y., Su Y., Lu Y., Lian J., Li G. Composite microstructure and formation mechanism of calcium phosphate conversion coating on magnesium alloy. *Journal of The Electrochemical Society*. 2016;163(9): G138. https://doi.org/10.1149/2.0801609jes

31. JIA X., SONG J., QU X., ... PAN F. Effect of scratch on corrosion resistance of calciumphosphate conversioncoated AZ80 magnesium alloy. *Transactions of Nonferrous Metals Society of China*. 2022;32(1): 147–161. https://doi.org/10.1016/S1003-6326(21)65784-9

32. Jia X., Song J., Xiao B., ... Pan F. Influence of indentation size on the corrosion behaviour of a phosphate conversion coated AZ80 magnesium alloy. *Journal of Materials Research and Technology*. 2021;14: 1739–1753. https://doi.org/10.1016/j.jmrt.2021.07.091

33. Ong J. L., Chan D. C. N. Hydroxyapatite and their use as coatings in dental implants: A review. *Critical Reviews in Biomedical Engineering*. 2000;28(5&6): 667–707. https://doi.org/10.1615/CritRevBiomedEng.v28.i56.10

34. Dorozhkin S. V. Calcium orthophosphate coatings on magnesium and its biodegradable alloys. *Acta Biomaterialia*. 2014;10(7): 2919–2934. https://doi.org/10.1016/j.actbio.2014.02.026

35. Duan G., Yang L., Liao S., ... Wang F. Designing for the chemical conversion coating with high corrosion resistance and low electrical contact resistance on AZ91D magnesium alloy. *Corrosion Science*. 2018;135: 197–206. https://doi.org/10.1016/j.corsci.2018.02.051

36. Su Y., Guo Y., Huang Z., ... Ren L. Preparation and corrosion behaviors of calcium phosphate conversion coating on magnesium alloy. *Surface and Coatings Technology*. 2016;307(part A): 99–108. https://doi.org/10.1016/j.surfcoat.2016.08.065

37. Sun R. X., Wang P. F., Zhao D. D., Sun Z. Z., Li C. Q., Chen K. Z. An environment-friendly calcium phosphate conversion coating on AZ91D alloy and its

corrosion resistance. *Materials and Corrosion*. 2015;66(4): 383–386. https://doi.org/10.1002/maco.201307424

38. Braga J. de O., Santos dos D. M. M., Cotting F., … Nunes E. H. M. Surface modification of magnesium with a novel composite coating for application in bone tissue engineering. *Surface and Coatings Technology*. 2022;433: 128078. https://doi.org/10.1016/j.surfcoat.2021.128078

39. Kawahara M, Kato-Negishi M. Link between aluminum and the pathogenesis of Alzheimer's disease: The integration of the aluminum and amyloid cascade hypotheses. *International Journal of Alzheimer's Disease*. 2011;8: 276393. https://doi.org/10.4061/2011/276393

40. Zhang S., Zhang X., Zhao C., … Bian Y. Research on an Mg-Zn alloy as a degradable biomaterial. *Acta Biomaterialia*. 2010;6(2): 626–640. https://doi.org/10.1016/j.biomaterials.2003.08.009

41. Khan F., Panigrahi S. K. Age hardening, fracture behavior and mechanical properties of QE22 Mg alloy. *Journal of Magnesium and Alloy*. 2015;3(3): 210–217. https://doi.org/10.1016/j.jma.2015.08.002

42. Rzychoń T., Szala J., Kiełbus A. Microstructure, castability, microstructural stability and mechanical properties of ZRE1 magnesium alloy. *Archives of Metallurgy and Materials*. 2012;57(1): 245–252. https://doi.org/10.2478/v10172-012-0018-3

Information about the authors

Andrei V. Paspelau, Researcher at the Department of Physical, Colloidal and Analytical Chemistry, Belarusian State Technological University (Minsk, Republic of Belarus).

https://orcid.org/0000-0002-1287-603X
andrei29088@mail.ru

Aliaksandr A. Kasach, Cand. Sci. (Chem.), Assistant at the Department of Chemistry, Technology of Electrochemical Productions and Electronic Engineering Materials, Belarusian State Technological University (Minsk, Republic of Belarus).

https://orcid.org/0000-0001-5522-2928
kasach2018@bk.ru

Aleksandr R. Tsyganov, Dr. Sci. (Agric.), Academician, First Vice-Rector, Belarusian State Technological University (Minsk, Republic of Belarus).

https://orcid.org/0000-0001-5521-5613
tziganov@belstu.by

Irina I. Kurilo, Cand. Sci. (Chem.), Associate Professor, Head at the Department of Physical, Colloidal and Analytical Chemistry, Belarusian State Technological University (Minsk, Republic of Belarus).

https://orcid.org/0000-0002-0016-6719
september@tut.by

Received 28.09.2023; approved after reviewing 04.12.2023; accepted for publication 15.12.2023; published online 01.10.2024.

Translated by Yulia Dymant